



Article

# Correlated Target Search by Vaccinia Virus Uracil–DNA Glycosylase, a DNA Repair Enzyme and a Processivity Factor of Viral Replication Machinery

Evgeniia A. Diatlova<sup>1</sup>, Grigory V. Mechetin<sup>1</sup>, Anna V. Yudkina<sup>1</sup>, Vasily D. Zharkov<sup>2</sup>, Natalia A. Torgasheva<sup>1</sup>, Anton V. Endutkin<sup>1</sup> , Olga V. Shulenina<sup>3</sup>, Andrey L. Konevega<sup>3</sup> , Irina P. Gileva<sup>4</sup>, Sergei N. Shchelkunov<sup>4</sup> and Dmitry O. Zharkov<sup>1,5,\*</sup>

<sup>1</sup> SB RAS Institute of Chemical Biology and Fundamental Medicine, 8 Lavrentieva Ave., 630090 Novosibirsk, Russia; e.diatlova@g.nsu.ru (E.A.D.); mechetin@niboch.nsc.ru (G.V.M.); ayudkina@niboch.nsc.ru (A.V.Y.); ashatan.314@gmail.com (N.A.T.); aend@niboch.nsc.ru (A.V.E.)

<sup>2</sup> Biology Department, Tomsk State University, 634050 Tomsk, Russia; arthropodae01@gmail.com

<sup>3</sup> NRC “Kurchatov Institute”—B. P. Konstantinov Petersburg Nuclear Physics Institute, Leningrad Region, 188300 Gatchina, Russia; ovshulenina@gmail.com (O.V.S.); konevega\_al@pnpi.nrcki.ru (A.L.K.)

<sup>4</sup> State Research Center of Virology and Biotechnology Vector, Novosibirsk Region, 630559 Koltsovo, Russia; gileva@vector.nsc.ru (I.P.G.); snshchel@rambler.ru (S.N.S.)

<sup>5</sup> Department of Natural Sciences, Novosibirsk State University, 2 Pirogova St., 630090 Novosibirsk, Russia

\* Correspondence: dzharkov@niboch.nsc.ru; Tel.: +7-383-363-5187; Fax: +7-383-363-5128



**Citation:** Diatlova, E.A.; Mechetin, G.V.; Yudkina, A.V.; Zharkov, V.D.; Torgasheva, N.A.; Endutkin, A.V.; Shulenina, O.V.; Konevega, A.L.; Gileva, I.P.; Shchelkunov, S.N.; et al. Correlated Target Search by Vaccinia Virus Uracil–DNA Glycosylase, a DNA Repair Enzyme and a Processivity Factor of Viral Replication Machinery. *Int. J. Mol. Sci.* **2023**, *24*, 9113. <https://doi.org/10.3390/ijms24119113>

Academic Editors: David Alexander Forsyth Gillespie and Ingrid Tessmer

Received: 20 April 2023

Revised: 13 May 2023

Accepted: 21 May 2023

Published: 23 May 2023



**Copyright:** © 2023 by the authors. Licensee MDPI, Basel, Switzerland. This article is an open access article distributed under the terms and conditions of the Creative Commons Attribution (CC BY) license (<https://creativecommons.org/licenses/by/4.0/>).

**Abstract:** The protein encoded by the vaccinia virus *D4R* gene has base excision repair uracil–DNA *N*-glycosylase (vvUNG) activity and also acts as a processivity factor in the viral replication complex. The use of a protein unlike PolN/PCNA sliding clamps is a unique feature of orthopoxviral replication, providing an attractive target for drug design. However, the intrinsic processivity of vvUNG has never been estimated, leaving open the question whether it is sufficient to impart processivity to the viral polymerase. Here, we use the correlated cleavage assay to characterize the translocation of vvUNG along DNA between two uracil residues. The salt dependence of the correlated cleavage, together with the similar affinity of vvUNG for damaged and undamaged DNA, support the one-dimensional diffusion mechanism of lesion search. Unlike short gaps, covalent adducts partly block vvUNG translocation. Kinetic experiments show that once a lesion is found it is excised with a probability ~0.76. Varying the distance between two uracils, we use a random walk model to estimate the mean number of steps per association with DNA at ~4200, which is consistent with vvUNG playing a role as a processivity factor. Finally, we show that inhibitors carrying a tetrahydro-2,4,6-trioxypyrimidinylidene moiety can suppress the processivity of vvUNG.

**Keywords:** DNA repair; uracil–DNA glycosylase; protein translocation; viral replication; processivity; correlated cleavage; random walk; vaccinia virus; protein targeting

## 1. Introduction

Base excision DNA repair (BER) is an important protective pathway keeping the genomes of living cells free of deaminated, oxidized, and alkylated bases, apurinic/aprimidinic (AP) sites, and single-strand breaks [1,2]. When a damaged base is present, BER is initiated by one of several DNA glycosylases, the enzymes that specifically recognize a damaged base and hydrolyze its *N*-glycosidic bond [2,3]. The formed AP site is then processed via several subpathways involving AP endonucleases, DNA polymerases, DNA ligases, and a host of accessory proteins. DNA glycosylases usually possess general specificity for purine or pyrimidine bases damaged in chemically similar ways, e.g., for oxidized purines or ring-alkylated purines [1–3]. In their search for sites of DNA damage, DNA glycosylases employ the facilitated diffusion mechanism (often termed “processive search”) based on association with non-specific DNA and random one-dimensional diffusion to survey a

short segment (tens to hundreds of nucleotides) for the presence of a lesion [4–6]. The opposite of processive search is distributive search, where the protein binds and releases DNA without significant lateral movement until it happens to encounter the target.

Uracil, one of the most abundant types of DNA damage, arises from cytosine deamination, either spontaneous or catalyzed by cytosine deaminases, and appears in the genome through either direct damage to C in DNA or incorporation of dUMP from the pool of residual metabolic dUTP or damaged dCTP [7,8]. Hydrolytic C deamination is unavoidable in aqueous solution and thus affects every living being. U is removed from DNA through the action of uracil–DNA glycosylases (UNG), the enzymes universally found throughout cellular life and in some viruses with DNA genomes. Human cells, for example, possess four enzymes capable of U excision: UNG, single-strand selective monofunctional uracil–DNA glycosylase (SMUG1), G/T mismatch-specific thymine–DNA glycosylase (TDG), and methyl–CpG-binding domain protein 4 (MBD4). Of these, UNG, SMUG1, and TDG belong to the same structural superfamily sharing the  $\alpha/\beta$ -fold. UNG, which seems to be the primary U-removing enzyme, is associated with the replication fork and is cell-cycle-regulated, while SMUG1 likely contributes to the protection of the genome from U formation outside of the S phase [8,9].

While UNG superfamily members can be found in nearly every cellular genome sequenced so far, the role of these enzymes and U repair in general in the life cycle of viruses remains poorly characterized. UNG homologs are widely present in the genomes of herpesviruses, poxviruses, many giant viruses (e.g., Mimivirus, Pandoravirus, and Pithovirus), and a limited number of bacteriophages. However, the necessity of UNG for replication or infectivity was only demonstrated for some herpesviruses [10–13] and poxviruses (see below). Viruses, of course, can subvert host cell DNA repair systems for their own use; this strategy is used by human immunodeficiency virus 1 which incorporates host UNG into the viral particles to protect its cDNA genome from mutations [14–16].

Poxviruses are among a few groups of viruses requiring the presence of uracil–DNA glycosylases for their replication. Poxviruses encode their own UNG protein (*D4R* gene in the vaccinia virus strain Copenhagen genome; below, we refer to the vaccinia virus protein as vvUNG), and its deletion drastically decreases the ability of the virus to replicate in cells [17–19]. The enzymatic properties of vvUNG and its close relative, monkeypox virus UNG, have been partially characterized, revealing fairly typical UNG kinetics, substrate specificity, and buffer requirements but resistance to the inhibiting action of Ugi, a small phage protein tightly binding to UNG [20,21]. The structure of vvUNG has been solved both alone and bound to normal DNA, damaged DNA, and viral A20 protein that does not bind DNA but tethers vvUNG to the viral replication complex [22–30].

There are conflicting data as to whether the viability of poxviruses depends on the repair function of their UNG. Some studies reported that selective inactivation of DNA glycosylase function by site-directed mutagenesis leads to suppression of replication [19], while others claim that the replication is supported by mutant forms of the enzyme lacking catalytic activity [31]. It is known that UNG-deficient vaccinia virus can only replicate in cells ectopically expressing vvUNG but not the host UNG [32,33]. The virulence of vaccinia virus strain carrying mutations in the vvUNG active site in mice is sharply reduced [31]. It has been suggested that, instead of DNA repair, the main role of UNG in poxviral replication may be imparting processivity to viral DNA polymerase, since the heterodimer of DNA-binding D4 and bridging A20 proteins acts a processivity subunit of the poxvirus DNA replication complex [23,34]. However, the processivity of vvUNG or UNG from any other poxviral species has never been studied. Notably, structures of vvUNG indicate that, unlike PolN/PCNA sliding clamps, it does not fully close around DNA, so it is unclear whether its intrinsic processivity can support viral replication.

To assess the processivity of BER enzymes in a quantitative way, we [35] and others [36,37] independently developed a method for kinetic analysis based on the probability of correlated cleavage ( $P_{cc}$ ; see Supplementary Text for a formal description) of substrates containing a pair of damaged sites separated by variable distances. Essentially, the probabil-

ity of transfer between two sites without releasing DNA is taken as a measure of processive lesion search. Using a random walk model on a one-dimensional lattice (e.g., [38]), one can then estimate the biologically relevant parameters such as the average survey length. Since then, the approach has been applied to estimate the processivity of human and *E. coli* UNG (hUNG and EcoUng, respectively), 8-oxoguanine–DNA glycosylases Fpg and OGG1, alkylpurine–DNA glycosylases AlkA and MPG, and AP endonucleases Nfo and APEX1 [35–37,39–53]. In this work, we quantitatively characterize the lesion search by vvUNG and conclude that its intrinsic ability for one-dimensional diffusion along DNA is indeed compatible with the role of this protein as a polymerase processivity factor.

## 2. Results

### 2.1. vvUNG Is Capable of Correlated DNA Cleavage

Correlated cleavage of substrates containing two U bases reflects the ability of UNG enzymes to move from one lesion to another without releasing the bound DNA [35,37]. In DNA-binding proteins, the physical basis of such movement can be either movement along the helical axis without losing the essential contacts with DNA (sliding) or short-distance dissociation/association events without bulk rehydration of the protein–DNA interface (hopping) [54–56]. In any case, the correlated search characteristically depends on the ionic strength of the solution, reflecting the mostly electrostatic nature of protein–DNA interactions and the need to expel bound ions from the interface upon lateral movement.

Using a double-stranded substrate with two U residues located in the identical sequence context and separated by 19 nt of undamaged intervening sequence, we followed the accumulation of products cleaved at one site and at both sites (Figure 1a–c). For the correlated cleavage experiments, a large excess (>400-fold) of the substrate was taken to minimize independent cleavage at both sites, and only the linear parts of the product accumulation time courses were considered to ensure steady-state conditions. The efficiencies of U excision from 20-mer duplex substrates corresponding to each individual half of the construct were determined in separate experiments and were found to be similar (Supplementary Figure S1; U20L//G20L:  $K_M = 400 \pm 140$  nM,  $k_{cat} = 5.8 \pm 0.8$  s<sup>-1</sup>; U20R//G20R:  $K_M = 330 \pm 80$  nM,  $k_{cat} = 7.3 \pm 0.5$  s<sup>-1</sup>). When the reaction mixture contained only 25 mM Tris–HCl (approx. 20 mM in monovalent cations at 37 °C and pH 7.5) and low concentrations of EDTA and DTT, about 70% of cleavage events at one site were followed by cleavage at the second site (Figure 1d). However, a gradual increase in salt (KCl) concentration up to 200 mM drastically decreased  $P_{cc}$ , consistent with the mechanism dependent on protein one-dimensional diffusion along DNA (Figure 1d). Notably, vvUNG showed higher  $P_{cc}$  values than EcoUng at any KCl concentration (Supplementary Figure S2). Substituting MgCl<sub>2</sub> for KCl had an even larger effect, with the cleavage being almost fully distributive already at 10 mM (Figure 1d). This is not surprising given the much tighter binding of Mg<sup>2+</sup> ions to DNA compared with monovalent cations. Even when the total ionic strength of the solution was taken into account, MgCl<sub>2</sub> still was more detrimental for the correlated cleavage (Supplementary Figure S3a). This effect was not due to better stability of the duplex in the presence of divalent cations, since when  $P_{cc}$  was plotted against the equivalent cation concentration (i.e., the concentrations of Mg<sup>2+</sup> and K<sup>+</sup> that stabilize duplex DNA equally [57]), MgCl<sub>2</sub> had less influence on the correlated cleavage than KCl (Supplementary Figure S3b). Thus, the more pronounced effect of MgCl<sub>2</sub> is likely due to its tighter binding to DNA that complicates Mg<sup>2+</sup> displacement by the moving protein.

UNG enzymes, including vvUNG, are known to excise U from single- and double-stranded DNA [20,58,59]. Moreover, the ability of EcoUng to perform correlated cleavage of a double-stranded substrate is not compromised by intervening single-stranded gaps up to 6 bp in length [41]. We inquired into whether vvUNG can bypass nicks and short gaps (2, 4, or 6 nt) without releasing DNA. The values of  $P_{cc}$  were similar in all cases (Figure 2a), indicating that single-stranded DNA gaps do not represent an obstacle for moving vvUNG.

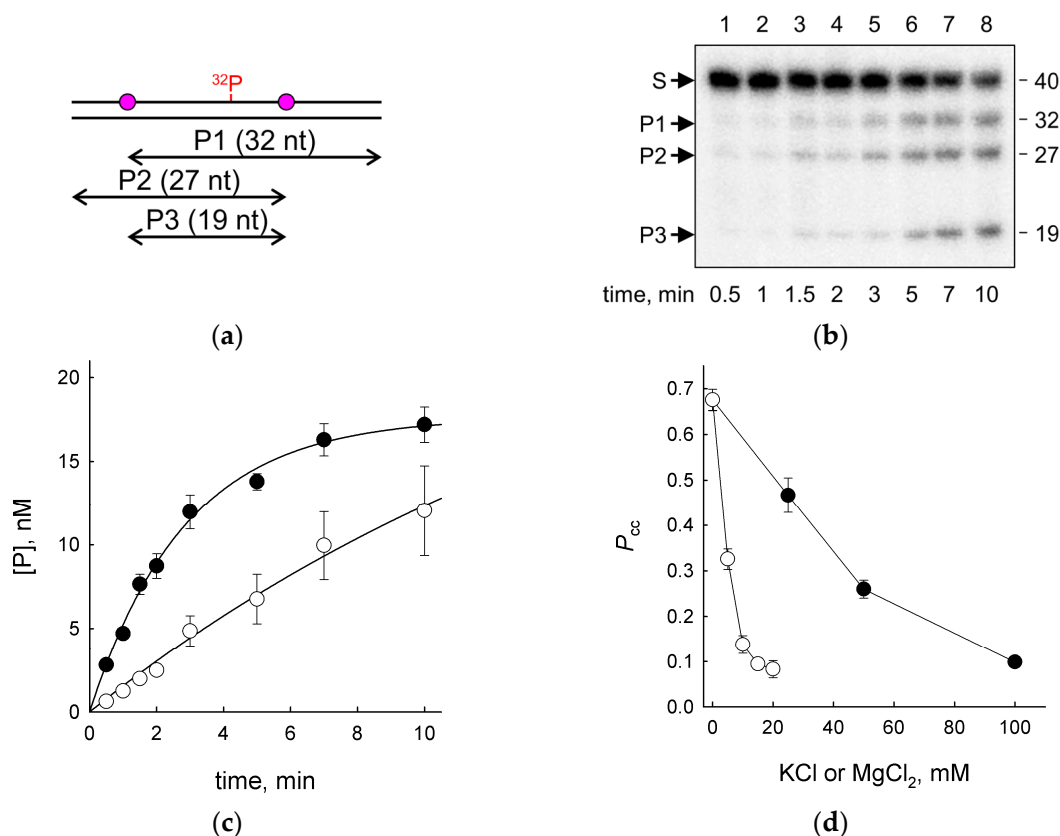


**Figure 1.** Correlated cleavage of DNA carrying two U bases by vvUNG. (a) Scheme of the substrate. Purple circles correspond to the lesions;  $^{32}\text{P}$  marks the position of the radioactive label. P1, P2, and P3 are the cleavage products with their respective lengths. (b) Representative gel image showing the accumulation of cleavage products with time. Arrows: S, substrate; P1–P3, cleavage products as in Panel A. Lengths of the substrate and the products are marked next to the gel. (c) Time course of product accumulation (25 mM KCl). Closed circles, P1 + P2; open circles, P3. (d) Dependence of  $P_{cc}$  on the concentration of KCl (closed circles) and  $\text{MgCl}_2$  (open circles). Mean  $\pm$  SD of three independent experiments is shown in (c,d).

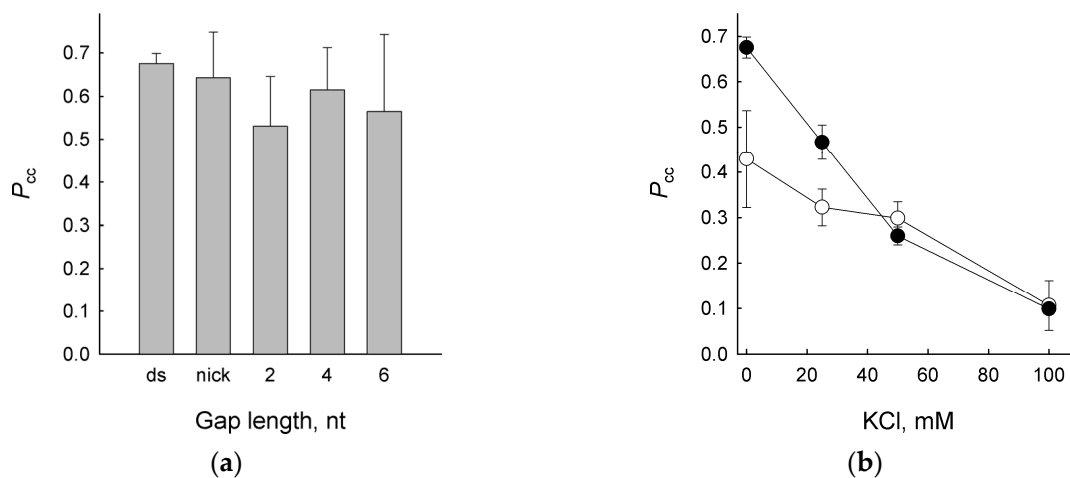


**Figure 2.** Correlated cleavage by vvUNG with nicks or gaps (a) or a bulky fluorescein residue (b) between two U residues. Mean  $\pm$  SD of three independent experiments is shown. In (a), ds, uninterrupted duplex; nick, duplex lacking a single phosphate. In (b), closed circles are  $P_{cc}$  values for the internally  $^{32}\text{P}$ -labeled substrate, open circles are  $P_{cc}$  values for the fluorescein-labeled substrate.

Introduction of a bulky group such as fluorescein into the DNA duplex interferes with the one-dimensional diffusion ability of EcoUng [52]. Replacing the [ $^{32}\text{P}$ ]-phosphate label between the damaged sites with a fluorescein moiety tethered to T through an aminohexyl-3-acrylimide linker significantly reduced the  $P_{cc}$  of vvUNG at low salt concentrations but had a much less pronounced effect at  $\geq 50$  mM KCl (Figure 2b). This observation is consistent with the dominating effect of a sliding mechanism of vvUNG at low salt.

We also compared the correlated cleavage in substrates containing 19 or 20 undamaged nucleotides between the lesions as a check for the effect of the rotation phase around the helical axis. If the moving protein tracks a DNA groove, the differences in  $P_{cc}$  will be minimal, whereas if it moves along the linear axis, one could expect larger differences due to the helical twist that displaces the adjacent nucleotides by  $36^\circ$  in B-DNA [60]. The difference between the  $P_{cc}$  values was indeed minor ( $0.67 \pm 0.02$  for the 19 nt distance,  $0.65 \pm 0.05$  for the 20 nt distance), again consistent with the movement along the DNA groove.

## 2.2. vvUNG Binds Damaged and Undamaged DNA with Similar Affinity

To clarify the origins of efficient transfer of vvUNG along DNA, we have used microscale thermophoresis to measure the affinity of vvUNG for single- and double-stranded DNA, both undamaged and containing (3-hydroxytetrahydrofuran-2-yl)methyl phosphate (F), an AP site analog mimicking the product of the DNA glycosylase reaction. Binding of vvUNG to oligonucleotide ligands 5'-labeled with the Cy3 dye produced clearly visible changes in the thermal diffusion of the complex (Figure 3a). The affinity of vvUNG for single-stranded undamaged DNA, double-stranded undamaged DNA, F-containing single-stranded DNA, and double-stranded DNA with F:G or F:A pairs was in the same order of magnitude, ranging from  $4 \mu\text{M}$  to  $12 \mu\text{M}$  (Figure 3b, Table 1). F-containing ligands were bound somewhat better, but the preference for the damaged DNA was at most threefold (Table 1) indicating that vvUNG possesses a rather uniform ability to bind any DNA, as would be expected of a processivity factor.

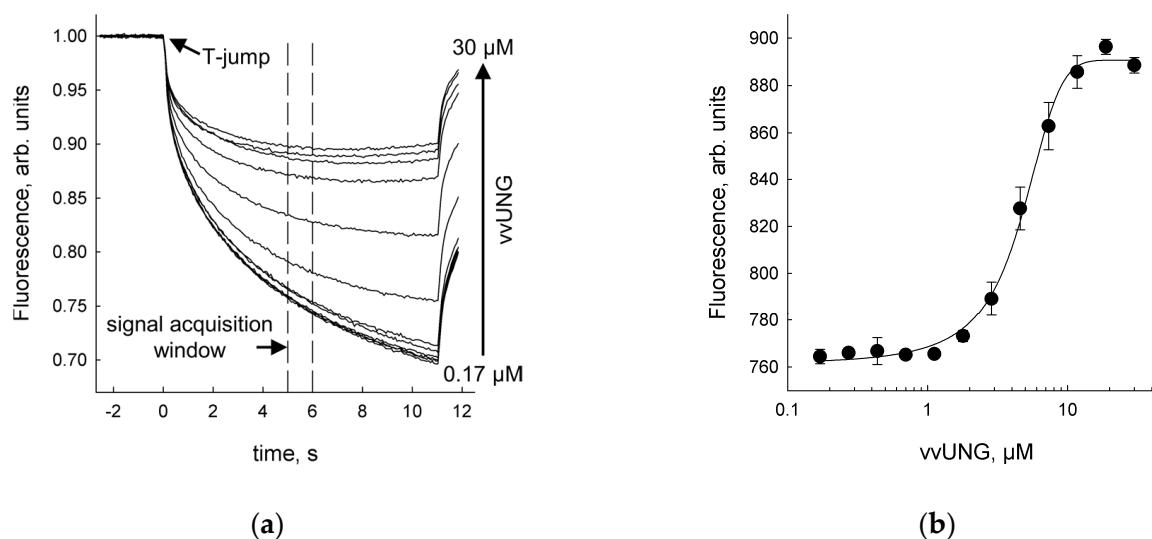


**Figure 3.** Binding of vvUNG to DNA followed by microscale thermophoresis. (a) Representative set of fluorescence traces for the C:G ligand. (b) Binding curve for the C:G ligand. Mean  $\pm$  SD of three independent experiments is shown.

The  $K_d$  values found here are severalfold higher than those reported for EcoUng non-specific binding to double-stranded DNA ( $1\text{--}1.5 \mu\text{M}$ ) [37,61]. However, since our experiments were performed at higher salt concentrations, with a shorter duplex, and using a different assay, it can be assumed that the general binding affinities of vvUNG and EcoUng for non-specific DNA duplex are comparable.

**Table 1.** vvUNG affinity for normal and damaged DNA.

Substrate (Oligo IDs)	$K_d$ , $\mu\text{M}$ <sup>a</sup>
C (13C)	$7.0 \pm 2.0$
T (13T)	$12 \pm 7$
F (13F)	$4.0 \pm 2.0$
C:G (13C//13cmpG)	$7.2 \pm 1.5$
T:A (13T//13cmpA)	$8.7 \pm 1.7$
F:G (13F//13cmpG)	$6.2 \pm 2.3$
F:A (13F//13cmpA)	$6.7 \pm 1.4$

<sup>a</sup> Mean  $\pm$  SD of three independent experiments.

### 2.3. Efficiency of Lesion Recognition by vvUNG

The probability of correlated cleavage  $P_{cc}$  is a product of two factors: the probability of transfer from one site to another ( $P_T$ ) and the probability of U excision upon encounter ( $P_E$ ) [37]. Thus, to single out the transfer probability, we determined  $P_E$  in a separate pulse-chase kinetic partitioning experiment. The scheme was essentially as described in [37,43] for hUNG and EcoUNG with minor modifications: we mixed vvUNG (2  $\mu\text{M}$ ) with the substrate (20 nM) in a rapid quench flow apparatus and 2.5 ms later either quenched the reaction with alkali to obtain the amount of the product already formed at the first technically achievable quench time, or chased with a trap (heparin) for up to 20 s (Figure 4a). After the trap was added at 2.5 ms, all the product formed later was derived in a single-turnover mode from the ES complex existing by that time. Extrapolation of the product accumulation to zero time, corrected for the amount of product already formed at 2.5 ms ( $6.1 \pm 1.0$  nM in our case), gave the amount of product formed from a single lesion-binding event. The ratio of this product ( $[P]^*$ ;  $10.6 \pm 1.1$  nM) to the extrapolated zero time substrate ( $[S]^*$ ;  $3.3 \pm 0.3$  nM) gave the ratio of the glycosidic bond cleavage rate ( $k_{ex}$ ) to the non-productive dissociation rate of the ES complex ( $k_{off}$ ) [37] (Figure 4b). From this, the excision probability  $P_E$  may be obtained as  $P_E = k_{ex}/(k_{ex} + k_{off}) = [P]^*/([P]^* + [S]^*)$ . For vvUNG, it was  $0.76 \pm 0.02$ , which is very close to the  $P_E = 0.73$  and  $0.81$  reported for EcoUng and hUNG, respectively [37,43]. This value was taken to calculate  $P_T$  from  $P_{cc}$  in the modeling exercise described in the next section.

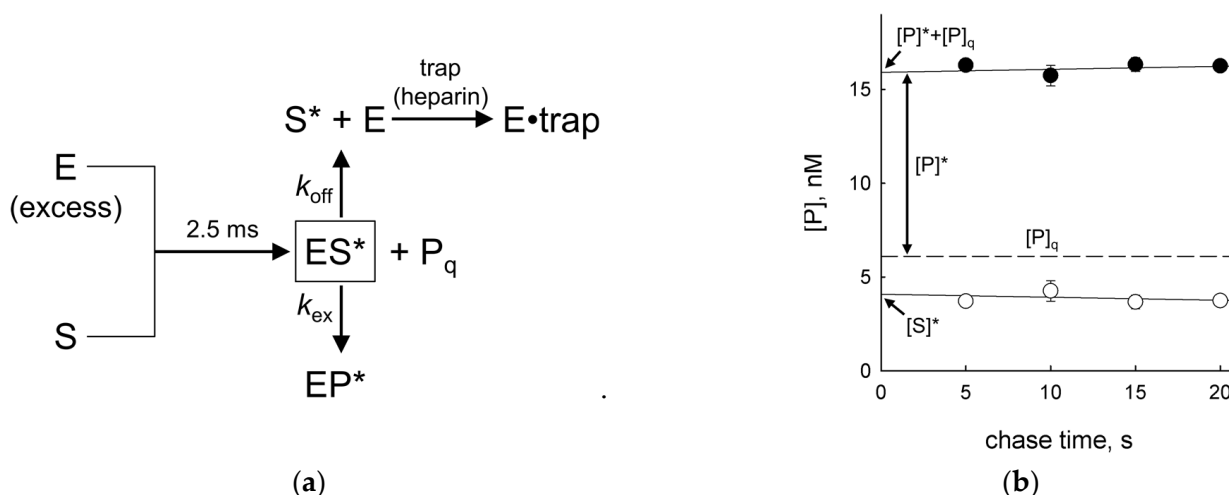


**Figure 4.** Excision efficiency of vvUNG measured in quench flow experiments. (a) General scheme of the experiment. (b) Accumulation of the product (closed circles) and consumption of the substrate (open circles) during the chase.  $P_q$ , product formed within 2.5 ms;  $P^*$ , product formed during the chase period;  $S^*$ , substrate remaining during the chase period. Mean  $\pm$  SD of three independent experiments is shown.

#### 2.4. Dependence of $P_{cc}$ on the Distance between the Lesions

In order to estimate the effective survey distance using vvUNG, we have constructed a series of substrates in which two U residues were separated by non-damaged intervening sequences of different lengths (19, 20, 40, 60, or 80 normal nucleotides between the lesions). When conducting the search, the enzyme could fall off the DNA either from an internal position or from one of the ends, and the fraction of the enzyme that reached the second site decreased with wider separation between the lesions [38,43]. Indeed, the efficiency of the intersite transfer dropped sharply when the distance increased from 20 nt to 40 nt and then continued to decrease less sharply, in total descending from  $0.67 \pm 0.02$  at a distance of 19 nt to  $0.20 \pm 0.03$  at a distance of 80 nt (Figure 5a). Notably, these  $P_{cc}$  values were always higher than the values for EcoUng obtained in the same substrate system under the same conditions [41] where  $P_{cc}$  dropped from 0.39 with 20 nt separating the damaged sites to 0.12 with 80 nt separating the damaged sites (Supplementary Figure S4).

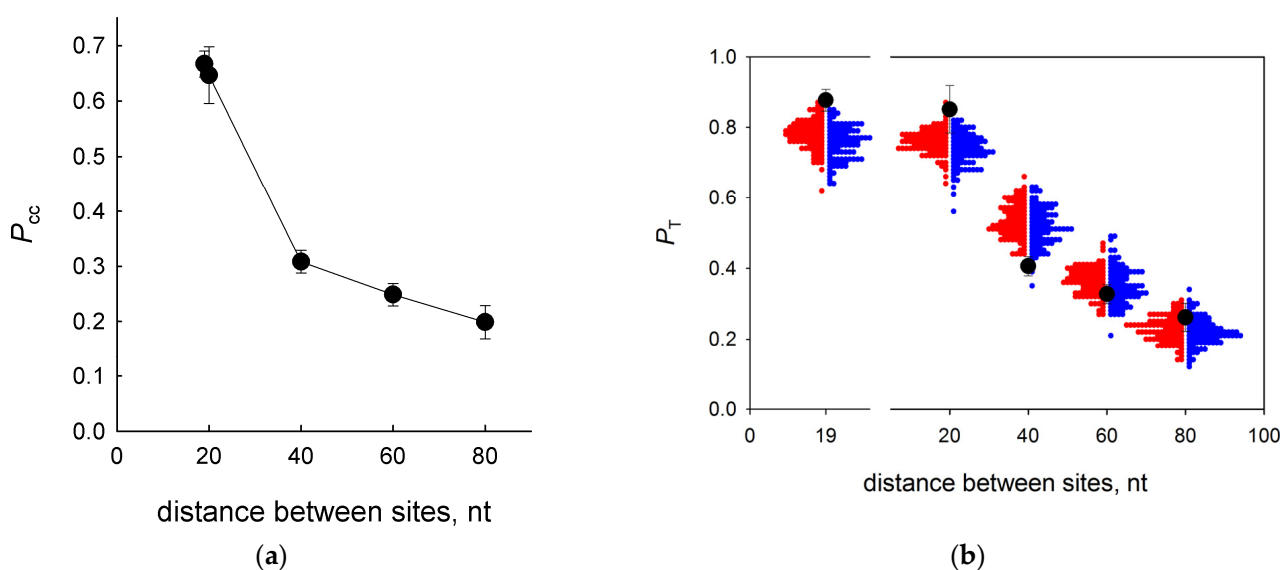


**Figure 5.** (a) Dependence of vvUNG  $P_{cc}$  on the distance between the U residues. Mean  $\pm$  SD of three independent experiments is shown. (b) Simulation of vvUNG random walk on a finite one-dimensional grid with irreversible losses. Black symbols are experimental  $P_T$  data used for fitting. Colored dots show the fraction of successful walks from position 8 to positions 28, 29, 49, 69 or 89 (red dots) or from positions 28, 29, 49, 69 or 89 to position 8 (blue dots).

In previous studies employing the two-site cleavage assay, estimates of the biologically relevant parameters of EcoUng one-dimensional diffusion were made analytically using available models of a one-dimensional random walk [37,41,43]. Here, we used an alternative approach, namely the simulation of a one-dimensional random walk with losses, to evaluate the microscopic characteristics of vvUNG processivity. We employed a simple model of a single-node-size particle walking in discrete steps along a finite one-dimensional grid, with each step carrying a probability of irreversible loss from an internal node  $p_{off}$  and a larger probability of irreversible loss from a terminal node  $p_{off} + p_{end}$ . The estimates of  $p_{off}$  and  $p_{end}$  were made from fitting simulated walks on grids whose lengths and start and finish node position corresponded to the actual substrates ( $\sim 3 \times 10^9$  walks in total) to the experimental  $P_T$  data (see Materials and Methods for a detailed description). Initially, we benchmarked the simulations against the experimental data for EcoUng and the estimates made from these data using the Belotserkovskii–Zarling analytical approximation of a random walk with losses [38]. The simulation produced the values of  $p_{off} = (4.99 \pm 0.64) \times 10^{-5}$  and  $p_{end} = 0.179 \pm 0.004$  (mean  $\pm$  s.e.m.), in reasonable agreement with  $p_{off} \sim 1 \times 10^{-4}$  and  $p_{end} = 0.17$  as reported in [41] (Supplementary Figure S5). The distribution of successive walks in the opposite directions was notably asymmetric due to high  $p_{end}$  and differ-

ent lengths between the ends and the start and finish nodes (Supplementary Figure S5). Global fitting of the simulation to the experimental data for vvUNG (Figure 5b) quite unexpectedly produced a  $\sim 5$ -fold higher  $p_{\text{off}} = (2.41 \pm 0.07) \times 10^{-4}$  and a  $\sim 30$ -fold lower  $p_{\text{end}} = (6.06 \pm 0.33) \times 10^{-3}$  (mean  $\pm$  s.e.m.) in comparison with EcoUNG. This, in particular, may indicate that the physical processes underlying the off-rate estimates for EcoUNG from  $K_d$  experiments with short non-specific oligonucleotide substrates [37,61] could be different from those for DNA release by vvUNG. Notably, the model underestimated  $P_{\text{cc}}$  at the shortest intersite distances, indicating the possibility of enhanced transfer at the  $\sim 20$ -nt range. However, alternative walk models that also entailed short-distance hopping or pauses in sliding produced quantitatively similar results, so the nature of this enhanced transfer remains to be established.

### 2.5. Small-Molecule Inhibitors Affecting Correlated Cleavage by vvUNG

Recently, we identified a series of low-molecular-weight compounds with modest inhibitory properties ( $\text{IC}_{50} \sim 10\text{--}100 \mu\text{M}$ ) towards vvUNG [62]. These inhibitors are derived from the tetrahydro-2,4,6-trioxypyrimidinylidene (PyO3) moiety and, according to molecular docking, occupy the uracil-binding pocket of UNG and form additional contacts near its entrance. Here, we addressed the effect of these inhibitors on correlated cleavage by vvUNG. Since  $P_{\text{cc}}$  is calculated as a ratio of initial reaction rates, a decrease in  $v_0$  at the individual U sites due to inhibitor binding does not affect  $P_{\text{cc}}$ , and any observable effect is due to a change in the intersite transfer efficiency. We used three compounds from the screened library (Figure 6a), of which compound 2F demonstrated no inhibitory properties, whereas compounds 2D and 3A were inhibitors ( $\text{IC}_{50} \sim 120 \mu\text{M}$  and  $70 \mu\text{M}$ , respectively) [62]. No change in  $P_{\text{cc}}$  was observed with 2F up to  $1000 \mu\text{M}$ . 2D caused a  $\sim 15\%$  decrease in  $P_{\text{cc}}$  at the highest concentration used ( $1000 \mu\text{M}$ ; Figure 6b). The effect of 3A was more pronounced:  $P_{\text{cc}}$  dropped by  $\sim 15\%$  at  $100 \mu\text{M}$  and by  $37\%$  at  $1000 \mu\text{M}$  compound 3A (Figure 6b). Although the magnitude of the effect is moderate, these results show that intersite transfer can be suppressed by low-molecular-weight compounds that presumably compete with DNA for contacts in or near the enzyme's lesion-binding site.

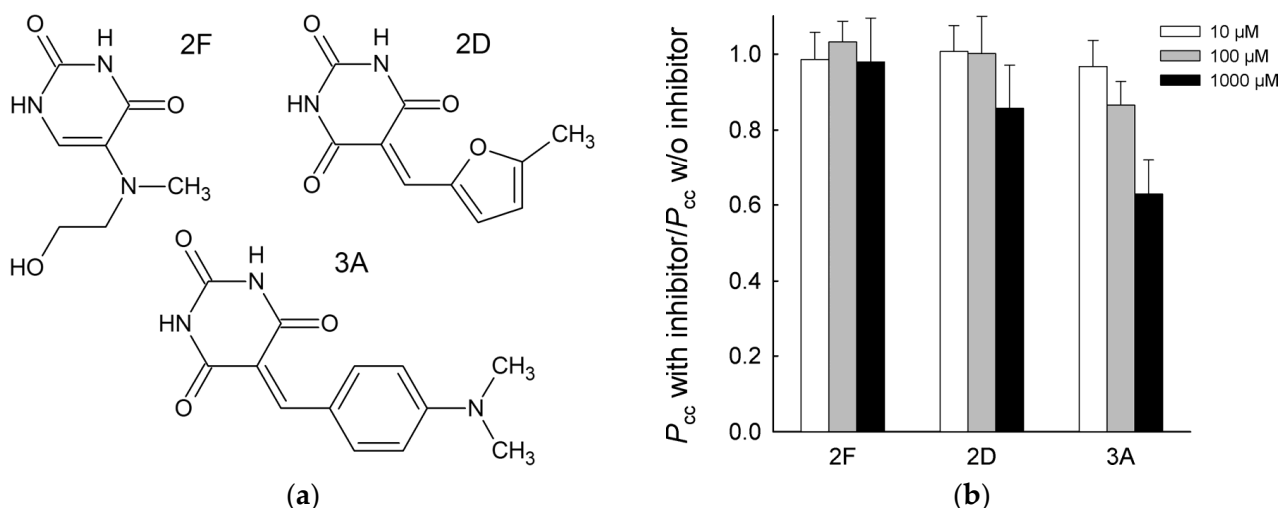


**Figure 6.** Inhibition of correlated cleavage by PyO3 derivatives. (a) Structures of the compounds 2D, 2F, and 3A. (b) Dependence of  $P_{\text{cc}}$  (normalized for  $P_{\text{cc}}$  without the inhibitor) on the inhibitor concentration. Mean  $\pm$  SD of three independent experiments is shown.

### 3. Discussion

DNA glycosylases are key members of the network safeguarding the genome from endogenous and environmental damage. There are rare occurrences of DNA glycosylases that, while maintaining the same catalytic chemistry, have evolved to play a role in other cellular processes. The best-known examples are thymine–DNA glycosylases (TDG) in



vertebrates and DEMETER-like 5-methylcytosine glycosylases in higher plants, which excise epigenetically modified pyrimidine bases and mainly participate in gene activity regulation and chromatin organization [63,64]. There is increasing evidence that mammalian 8-oxoguanine–DNA glycosylase OGG1 can serve as a transcription activator and a guanine nucleotide exchange factor for some regulatory small GTPases [65]. However, the role of vvUNG in the viral replication complex so far appears to be unique among DNA glycosylases.

In the vast majority of living organisms, the replication machinery relies on dimeric or trimeric doughnut-shaped clamps to ensure processive DNA synthesis [66]. In herpesviruses, UL42 and UL44 processivity factors are, respectively, monomers and dimers and do not fully encircle DNA but share the same “processivity fold” with canonical clamp proteins [67,68]. Other than vvUNG, the only known DNA polymerase processivity factor not belonging to the clamp superfamily is thioredoxin, a bacterial protein adopted as a processivity subunit by bacteriophage T7 DNA polymerase. Thioredoxin, however, does not seem to contact DNA directly but rather stabilizes a long polymerase loop that tracks along DNA [69–72]. Additionally, single-strand binding proteins, although not considered processivity subunits in a strict sense, often enhance the processivity of DNA polymerases and have been used toward this end in fusion constructs [73,74]. Moreover, fusions with non-specific DNA-binding protein Sso7d [75] and DNA-binding helix–hairpin–helix motifs [76,77] can improve DNA polymerase processivity. Almost all studied DNA glycosylases have the ability to move along DNA randomly in search of the damaged sites, yet only vvUNG is known to be important for replicative processivity. Thus, it was interesting to address the intrinsic processivity of vvUNG and see whether it is compatible with its role in the viral replication complex.

Single-molecule assays such as the tightrope assay have recently gained popularity in studies of the facilitated diffusion of DNA-binding proteins. However, the actual observed species in single-molecule experiments is usually not a protein molecule per se but a complex coupled to a quantum dot through an antibody, or a fusion with a fluorescent protein tag, which may skew the parameters obtained with relatively small proteins such as DNA glycosylases. Moreover, the DNA used in some types of such experiments is heavily saturated with an intercalating or minor groove binding dye for visualization, which may affect protein–DNA interactions. Last but not least, precise chemical modification of the substrate is complicated with long DNA used in single-molecule assays. Ensemble kinetic methods, while providing less direct access to the walk parameters, may better reflect the intrinsic properties of the proteins under study and easily allow the introduction of nicks, gaps, obstacles, and other substrate modifications useful for mechanistic studies. The glycosylase activity of vvUNG allowed us to apply a two-site cleavage kinetic assay to characterize the protein’s diffusion along DNA.

Overall, we found that vvUNG behaves as expected for a processive DNA glycosylase and is more processive than EcoUng: its  $P_{cc}$  was higher at the same KCl concentrations, and at the same intersite distances (Supplementary Figures S2 and S4). Similarly to EcoUng, vvUNG was able to traverse nicks and short gaps, most likely because its affinity for ssDNA and dsDNA was similar. Modeling the one-dimensional walk with the experimentally determined kinetic parameters arrived at a  $\sim 2.4 \times 10^{-4}$  per-step probability of enzyme loss, corresponding to a mean lifetime of  $-1/\ln(1 - p_{off}) \approx 4200$  steps per association. If the movement is unidirectional, as in a replication complex performing DNA synthesis, this will be equal to the mean displacement, or the average number of added nucleotides per association. Isolated vaccinia virus DNA polymerase is nearly distributive ( $\leq 10$  nt incorporated per binding event in 1 mM MgCl<sub>2</sub> or 40 mM NaCl) but, complete with the A20 and vvUNG subunits, it can replicate over a  $\sim 7000$  nt template in a single binding event [34,78,79]. Thus, the intrinsic processivity of vvUNG is in the same order of magnitude as the processivity of the full viral replication complex. It is quite possible that the fully assembled complex is more processive than its individual subunits. Assuming that the full complex is lost when both polymerase and vvUNG subunits are detached from DNA

simultaneously, and roughly estimating the per-step  $p_{\text{off}}$  for the isolated DNA polymerase at  $\sim 0.2$  (as  $(1 - 0.2)^{10} \approx 0.1$ , this would correspond to  $\sim 10\%$  polymerase molecules remaining bound after 10 nt incorporation and to  $\sim 4\text{--}5$  nt being incorporated per association), the combined  $p_{\text{off}} = p_{\text{off}}(\text{vvUNG}) \times p_{\text{off}}(\text{pol}) = 4.94 \times 10^{-5}$ , which translates to an average of  $\sim 21,000$  nucleotides per association. It should also be taken into account that, although the probability-based description of a random walk is by definition time-independent,  $p_{\text{off}}$  actually depends on the mean dwell time of a step (ultimately determined by the diffusion rate). In the replicative complex, the dwell time might be affected, leading to a change in  $p_{\text{off}}$  and the number of steps per association.

When we tried to extract microscopic parameters such as the probability of enzyme loss from an internal or a terminal position of linear DNA substrates, we found that a simple random one-dimensional walk model underestimates the vvUNG transfer at short ( $\sim 20$  nt) intersite distances. While the value of  $p_{\text{off}}$  produced by the numerical simulation is reasonable, being severalfold higher than that obtained for EcoUng, the higher-than-expected  $P_T$  at shorter distances may indicate the existence of additional processes beyond one-dimensional sliding. A similar phenomenon was observed by Porecha and Stivers for EcoUng [37] and was taken as evidence that hopping dominates over sliding at distances of  $>5\text{--}10$  nt. Moreover, the lack of strand dependence of cleavage [37] and inhibition of correlated cleavage by free uracil [43] are also more compatible with the hopping rather than sliding mechanism, assuming that enzyme reorientation on DNA or inhibitor binding cannot occur in the sliding mode. We also added short-distance hopping (with exponentially or power-law scaled probability) or pausing (essentially increasing the dwell time) to the walk scheme but this did not improve the outcome, with the hopping or pausing probabilities converging to nearly zero, while greatly lengthening the simulation. Hence, we did not pursue more complicated models at the time, and the relative contributions of sliding and hopping mechanism in the correlated target search by vvUNG remain to be addressed. Indirectly, the ability of vvUNG to traverse short gaps and the residual correlated cleavage in the presence of a bulky adduct (Figure 2) suggest that hopping indeed contributes to the lesion search. Interestingly, judging from the  $p_{\text{end}}$  values, vvUNG seems to be much less prone to a loss from the end of the duplex than EcoUng. Although this may be an artifact of the random walk model, the high affinity of vvUNG for DNA ends could be biologically meaningful, because the viral replicative complex has to remain or reassemble at the linear DNA terminus during reinitiation of self-priming hairpin replication [80,81].

One question relevant to vvUNG processivity is whether the isolated vvUNG protein is in the same form as vvUNG in the replicative complex. There is a certain discrepancy in the literature regarding the stoichiometry of vvUNG. The early structural studies of the isolated protein suggested that vvUNG exists as a dimer, and two dimerization interfaces were seen in crystal structures [22,23,25]. Notably, two interacting vvUNG molecules were observed in the crystal structure of a complex with undamaged DNA [28]. However, the most extensive interface observed in the isolated vvUNG homodimer was occupied by A20 in the replicative complex [26,29], and the 1:1:1 stoichiometry of binding of vvUNG, A20, and DNA polymerase [82,83] strongly suggests that the functional form of vvUNG as a processivity subunit is a monomer. In a recently determined cryo-EM structure of the monkeypox virus replicative complex, the three subunits were also found in a 1:1:1 ratio [84]. All other known DNA glycosylases are monomeric, and direct measurement of vvUNG mass in solution by analytical ultracentrifugation and size-exclusion chromatography suggests that the dimer appears only at high protein concentrations ( $\sim 10$  mg/mL) [26,30]. Thus, the functional glycosylase form of vvUNG in the cell and in our experiments is also likely monomeric.

Several amino acid substitutions in vvUNG are known to reduce the protein's ability to support processive DNA synthesis while retaining DNA glycosylase activity [23]. All of them affect basic residues located at the DNA-binding surface of the protein but distant from the active site pocket and are thus expected to perturb non-specific protein–DNA electrostatic interactions. The G179R mutation at the vvUNG/A20 interface also destabi-

lizes the interaction and results in a loss of processive DNA synthesis [34]. It appears that both the processivity of the vvUNG subunit and its proper coupling with the polymerase through A20 are important for the replication complex processivity.

The interface between vvUNG and the bridging A20 component of the poxviral replisome is an attractive target for the development of protein–protein interaction disruptors, a class of drugs actively pursued at present [85]. A number of hits that interfere with UNG from several poxviral species binding to A20 have been identified [86–90]. Notably, the assay used for the discovery of these molecules is based on the ability of the viral DNA polymerase to incorporate labeled dNMPs, which confirms the importance of the vvUNG/A20 interaction for the functionality of the polymerase complex. Our results, which show there is a possibility of direct suppression of the vvUNG processivity by low-molecular-weight compounds, point to an alternative mechanism that could be exploited to impede poxviral replication.

It remains to be seen how our *in vitro* quantitative results translate into the processivity of vvUNG and the viral replicative complex *in vivo*. Studying the mechanisms of lesion search in living cells is extremely challenging due to the fast timescale of the process, and only a handful of reports have been published for any DNA glycosylase in either bacteria or eukaryotes [51,91]. It is not known whether all vvUNG is sequestered in the viral replisome or exists partially as a free repair protein. Given that the vaccinia virus genome is AT-rich and, in addition to vvUNG, encodes a dUTPase [80,81], uracil may be an intrinsic problem for the virus, which vvUNG, with its efficient damage search mechanism, helps to alleviate in either a replication-coupled or replication-uncoupled manner. Our results add to the growing body of data suggesting that vvUNG may act as a viral replication processivity factor. In comparison with ubiquitous processivity clamps, vvUNG may seem less efficient: the size of the vaccinia virus genome is ~195 kb, so even the ~21 kb per association processivity estimate (see above) is likely insufficient for the replication complex to fully copy the genome without subunit exchange. On the other hand, poxviruses replicate in cytoplasmic factories, where the restricted volume might increase the concentration of vvUNG and the polymerase and facilitate reloading of the replicative complex to the released primer end, or re-association of isolated vvUNG to the scanned DNA. To our knowledge, there has been no direct estimate of vaccinia virus or other poxvirus replication processivity *in vivo*. Recently developed fluorescence-based methods allowing observation of polymerase exchange in living cells [92] could benefit the studies of viral replication processivity and clarify the role of vvUNG.

## 4. Materials and Methods

### 4.1. Enzymes, Oligonucleotides, and Chemicals

Restriction endonucleases and T4 DNA ligase were from Thermo Fisher Scientific (Waltham, MA, USA). Oligonucleotides were synthesized in-house from commercially available phosphoramidites (Glen Research, Sterling, VA, USA). The sequences are listed in Table 2. Oligonucleotides were 5'-labeled using  $\gamma$ [<sup>32</sup>P]-ATP (ICBFM Laboratory of Biotechnology, Novosibirsk, Russia) and T4 polynucleotide kinase (Biosan, Novosibirsk, Russia). Inhibitors were purchased from Vitas-M Chemical Ltd. (Hong Kong, China).

### 4.2. vvUNG Cloning and Purification

The *D4R* gene was cloned from the LIVP vaccinia virus strain (a derivative of the Lister strain) from the collection of the State Research Center of Virology and Biotechnology Vector [93]. The virus was grown on the CV-1 culture of African green monkey kidney cells, DNA was isolated using the QIAamp DNA Mini Kit (Qiagen, Venlo, The Netherlands), and the target gene was amplified using the pair of primers D4Rfwd and D4Rrev (Table 2). The PCR product was subcloned into pBluescript II SK(–), verified by sequencing, and the insert was recloned into the pET-15b expression vector at NdeI and XhoI sites. The resulting His<sub>6</sub>-tagged vvUNG (see Supplementary Text) was overexpressed in BL21(DE3) *E. coli* strain. The culture was grown in LB broth containing 100 µg/mL ampicillin at

37 °C until  $A_{595} = 0.8$ , then shifted to 25 °C and induced overnight with 0.5 mM isopropyl  $\beta$ -D-1-thiogalactopyranoside. All subsequent steps were conducted at 4 °C. The cells were harvested by centrifugation, the pellet was resuspended in the lysis buffer consisting of 10 mM Tris-HCl (pH 8.0), 1 mM EDTA, 500 mM NaCl, and 1 mM phenylmethylsulfonyl fluoride, and disrupted by sonication. The lysate was clarified by centrifugation at  $15,000 \times g$  for 20 min. The supernatant was treated with ammonium sulfate at 60% saturation for 2 h and precipitated at  $15,000 \times g$  for 20 min. The pellet was dissolved in Buffer A consisting of 20 mM Tris-HCl (pH 7.5) and 500 mM NaCl. The solution was filtered using 0.45  $\mu$ m syringe filters (MilliporeSigma, Burlington, MA, USA), loaded onto a 5 mL HisTrap column (GE Healthcare, Chicago, IL, USA) equilibrated in the same buffer, and purified using a 50–500 mM imidazole gradient. The fractions containing the target protein were identified by 12% SDS-PAGE (Laemmli system). The purest fractions, estimated as >95% homogeneous by Commassie Blue staining (Supplementary Figure S6), were pooled, aliquoted and stored at  $-80$  °C until use.

**Table 2.** Oligonucleotides used in this study.

Oligo ID	Sequence (5' → 3')
<i>D4R</i> gene cloning	
D4Rfwd	GGCATATGAATTCAGTACTGTATC
D4Rrev	GGGGATCCTAAAATTCACCTAAGC
Processivity studies	
U20L	TCCCTTCUCTCCTTTCCTTC
U20R	GGAATTCUCTCCTTTCAGCA
U21L	TCCCTTCUCTCCTTTCCTTCC
U40F <sup>1</sup>	TCCCTTCUCTCCTTTCCTTC[FluoT]GACTTCUCTCCTTTCAGCA
G17L	GGAAAGGAGGGAAGGGA
G17R	TCTGGAAAGGAGGGAAG
G18L	AGGAAAGGAGGGAAGGGA
G18R	TCTGGAAAGGAGGGAAGT
G19L	AAGGAAAGGAGGGAAGGGA
G19R	TCTGGAAAGGAGGGAAGTC
G20L	GAAGGAAAGGAGGGAAGGGA
G20R	TCTGGAAAGGAGGGAAGTCC
G40	TCTGGAAAGGAGGGAAGTCCGAAGGAAAGGAGGGAAGGGA
G40R	TCTGGAAAGGAGGGAAGTCCGAGGTCTGAACGAGAGGAAA
G41	TCTGGAAAGGAGGGAAGTCCGGAAGGAAAGGAGGGAAGGGA
G41L <sup>2</sup>	[p]GATCGCACAAATGAAAGGTCCGAAGGAAAGGAGGGAAGGGA
G46	TTTTCTGGAAAGGAGCGAAGTCCGAAGGAAAGGAGCGAAGGGATTT
G50L	[p]AAATTCATCATCGCACAAATGAAAGGTCCGAAGGAAAGGAGGGAAGGGA
G51R	TCTGGAAAGGAGGGAAGTCCGAGGTCTGAACGAGAGGAAAGCTAAATCCCC
G61	TCTGGAAAGGAGGGAAGTCCGCTCTAACGCAAGTAAAGTCCGAAGGAAAGGAGGGAAGGGA
L21	[p]GGACTTTACTTGCGTTAGAGC
L41	[p]GGACCTTTCATTTGTGCGATCTTTCCTCTCGTTCAGACCTC
L61	[p]GGACCTTTCATTTGTGCGATGAGTGAATTCGGGATTTAGCTTTCCTCTCGTTCAGACCTC
Microscale thermophoresis	
13C <sup>3</sup>	[Cy3]CCTTCCCTCCTTT
13T	[Cy3]CCTTCTCTCCTTT
13F	[Cy3]CCTTFCCTCCTTT
13cmpG	AAAGGAGGGAAGG
13cmpA	AAAGGAGAGAAGG

<sup>1</sup> [FluoT], fluorescein-dT <sup>2</sup> [p], synthetically introduced 5'-phosphate <sup>3</sup> [Cy3], synthetically introduced 5'-Cy3 dye.

#### 4.3. Substrate Preparation

For the steady-state kinetics on U20L and U20 halves, these were <sup>32</sup>P-labeled and annealed to a 1.5-fold molar excess of their respective complementary strands (G20L and G20R). Internally <sup>32</sup>P-labeled substrates for the correlated cleavage assay were prepared as

described previously [35,41] using the same general scheme: the right half of the substrate (U20R) was  $^{32}\text{P}$ -labeled at the 5'-end, mixed with a 1.5-fold molar excess of the left half (U20 or U21), the linker strand as needed (L21, L41, or L61), and one or two complementary strands (G40, G41, G61, G41L, G40R, G50L, G51R), depending of the length of the final substrate. After ligation, the duplexes were purified by non-denaturing electrophoresis in 8% or 12% polyacrylamide gel, desalted on a C18 Nensorb column (DuPont, Wilmington, DE, USA) and re-annealed. To prepare single-stranded U20L–U20R for gapped DNA experiments, the longer G46 strand was used as a ligation scaffold to ensure its complete separation by electrophoresis in a denaturing 20% polyacrylamide gel/8 M urea. Structures of all substrates are shown in Supplementary Figure S7.

#### 4.4. Steady-State Kinetics

The reaction mixture contained 50–2500 nM  $^{32}\text{P}$ -labeled substrate (U20L//G20L or U20R//G20R), 25 mM Tris–HCl (pH 7.5), 1 mM EDTA, 1 mM DTT, 0.1 mg/mL bovine serum albumin (BSA), and 0.12 nM vvUNG. After 5 min at 37 °C, aliquots were withdrawn, quenched by adding NaOH to 200 mM, heated for 2 min at 95 °C, neutralized with an equimolar amount of HCl, mixed with an equal volume of the gel loading solution (90% formamide, 0.05% bromophenol blue, 0.05% xylene cyanol), and heated again for 5 min. The reaction products were resolved by electrophoresis in 20% polyacrylamide gel/8 M urea and visualized by phosphorimaging (Typhoon FLA 9500 scanner, GE Healthcare). Steady-state kinetic parameters ( $K_M$  and  $k_{\text{cat}}$ ) were calculated from three independent experiments by non-linear fitting to a Michaelis–Menten equation using SigmaPlot v11.0 (Systat Software, Chicago, IL, USA).

#### 4.5. Correlated Cleavage Assay

The correlated cleavage assay protocols were similar to those described in [35,41]. The reaction mixture contained 50 nM substrate, 25 mM Tris–HCl (pH 7.5), 1 mM EDTA, 1 mM DTT, and 0.1 mg/mL BSA. Additionally, the mixture contained 10–200 mM KCl or 5–20 mM  $\text{MgCl}_2$  in the salt dependence experiments, and an inhibitor (10, 100 or 1000  $\mu\text{M}$ ) in the inhibition experiments. The reaction was initiated by adding vvUNG to 0.12 nM. After 0.5, 1, 1.5, 2, 3, 5, 7 and 10 min at 37 °C, aliquots were withdrawn and processed as described above. Initial reaction velocities were determined from the initial slopes of the reaction curves. The probability of correlated cleavage (see Supplementary Text) was estimated from three independent experiments as  $P_{\text{cc}} = v_{\text{P3}} / (v_{\text{P1}} + v_{\text{P2}} + v_{\text{P3}})$ , where  $v_{\text{P1}}$  and  $v_{\text{P2}}$  are rates of accumulation of the products of cleavage at one of the U sites, and  $v_{\text{P3}}$  is the rate of accumulation of the product of cleavage at both sites [35].

#### 4.6. Quench-Flow Experiments

The reactions were performed in a three-syringe rapid chemical quench apparatus RQF3 (KinTek, Snow Shoe, PA, USA) at 37 °C. The reaction mixture contained 20 nM  $^{32}\text{P}$ -labeled U20R//G20R substrate, 20 mM Tris–HCl (pH 7.5), 1 mM EDTA, 1 mM DTT, 0.1 mg/mL BSA, and 2  $\mu\text{M}$  vvUNG. The equal volumes of the enzyme and the substrate pre-diluted in the same buffer were mixed, and after 2.5 ms the reaction was quenched with 200 mM NaOH or chased with 3.8 mg/mL heparin. The reactions with the chaser were quenched in 5, 10, 15, or 20 s with 200 mM NaOH, then all the tubes were heated for 5 min at 95 °C and neutralized with an equimolar amount of HCl. The fractions were evaporated down to ~20  $\mu\text{L}$ , and the reaction products were resolved, visualized, and quantified as above. All time points were repeated 3–5 times.

#### 4.7. Microscale Thermophoresis

All reaction mixtures with a final volume of 10  $\mu\text{L}$  consisted of 50 nM Cy3-labeled oligonucleotide ligand, 0.17–30  $\mu\text{M}$  vvUNG, 20 mM Tris–HCl (pH 7.5), 50 mM KCl, 1 mM EDTA, 1 mM DTT, 5% (*v/v*) glycerol, and 0.05% Tween 20. Measurements were carried out using standard capillaries in the Monolith NT.115 device (NanoTemper Technologies,

Munich, Germany) in a red/green detection channel at medium infrared laser power. The data were fitted to a one-site ligand binding model using SigmaPlot v11.0.

#### 4.8. One-Dimensional Walk Simulation

On a finite one-dimensional grid of length  $L$  ( $L = 40, 41, 61, 81$  or  $101$ ) with two selected nodes, A (position 8) and B (position 28, 29, 49, 69 or 89), we modeled a random walk of a single-node-size particle that starts at either A or B, can be lost at each step from an internal node with a probability  $p_{\text{off}}$  and from a terminal node with a larger probability  $p_{\text{off}} + p_{\text{end}}$  (if  $p_{\text{off}} + p_{\text{end}} > 1$ , the combined probability of falling off the end in the simulation was taken for 1), and otherwise moves to any of the two adjacent grid nodes at each step with an equal chance. At the first iteration, a  $6 \times 6$  matrix with  $p_{\text{off}}$  and  $p_{\text{end}}$  values evenly spaced between 0 and 1 was generated. For each  $p_{\text{off}}, p_{\text{end}}$  pair we simulated 10,000 walks from A to B and 10,000 walks from B to A until either success (a completed walk between the selected nodes) or loss, and counted the number of successes for each bin of 100 walks. Thus, for every  $p_{\text{off}}, p_{\text{end}}$  pair 200 simulated transfer probabilities  $P_{\text{Tsim}}$  were obtained. The  $p_{\text{off}}, p_{\text{end}}$  pair producing the least sum of squares of differences from the experimentally determined  $P_{\text{T}}$  values,  $S = \sum (P_{\text{Tsim}} - P_{\text{T}})^2$ , over all simulations for all five grids, was carried into the next round, and the  $p_{\text{off}}$  and  $p_{\text{end}}$  values adjacent to the best pair in the matrix were taken as the bounds to generate a new  $6 \times 6$  matrix. The iterations were continued until the standard deviation of all  $S$  values in the matrix was less than 0.1 of  $S$  for the best  $p_{\text{off}}, p_{\text{end}}$  pair, which took 7–8 rounds. Ten such simulations were carried out, and the mean of the produced  $p_{\text{off}}$  and  $p_{\text{end}}$  values were taken as the final estimates. Lastly, with these  $p_{\text{off}}$  and  $p_{\text{end}}$ , 10,000 walks from A to B and 10,000 walks from B to A were simulated as above to obtain a distribution of  $P_{\text{Tsim}}$ . The whole procedure was implemented as a Python script available at [github.com/mizarium/MC\\_walk](https://github.com/mizarium/MC_walk).

**Supplementary Materials:** The following supporting information can be downloaded at <https://www.mdpi.com/article/10.3390/ijms24119113/s1>. References [94,95] are part of the Supplementary Materials.

**Author Contributions:** Conceptualization, D.O.Z.; methodology, E.A.D., G.V.M., A.V.Y., A.L.K., S.N.S. and D.O.Z.; software, A.V.Y., V.D.Z. and N.A.T.; validation, E.A.D. and G.V.M.; formal analysis, E.A.D. and D.O.Z.; investigation, E.A.D., V.D.Z., N.A.T., A.V.E., O.V.S. and I.P.G.; resources, A.L.K., S.N.S. and D.O.Z.; data curation, E.A.D. and N.A.T.; writing—original draft preparation, E.A.D.; writing—review and editing, S.N.S. and D.O.Z.; visualization, E.A.D. and D.O.Z.; supervision, A.L.K. and D.O.Z.; project administration, A.L.K. and D.O.Z.; funding acquisition, D.O.Z. All authors have read and agreed to the published version of the manuscript.

**Funding:** This research was supported by the Russian Science Foundation (grant 21-64-00017, all biochemical experiments) and the Russian Ministry of Higher Education and Science (grant 121031300056-8 to D.O.Z.). Quench-flow experiments were supported by the Russian Ministry of Higher Education and Science (grant 075-15-2021-1360 to A.L.K.).

**Institutional Review Board Statement:** Not applicable.

**Informed Consent Statement:** Not applicable.

**Data Availability Statement:** The script for modelling one-dimensional walks can be accessed at [github.com/mizarium/MC\\_walk](https://github.com/mizarium/MC_walk) (accessed on 20 May 2023). All other data are provided in the paper and the Supplementary Materials.

**Acknowledgments:** DNA sequencing was performed at the SB RAS Genomics Core Facility.

**Conflicts of Interest:** The authors declare that they have no conflict of interest with the contents of this article.

## References

1. Friedberg, E.C.; Walker, G.C.; Siede, W.; Wood, R.D.; Schultz, R.A.; Ellenberger, T. *DNA Repair and Mutagenesis*; ASM Press: Washington, DC, USA, 2006; p. 1118.
2. Zharkov, D.O. Base excision DNA repair. *Cell. Mol. Life Sci.* **2008**, *65*, 1544–1565. [[CrossRef](#)] [[PubMed](#)]
3. Stivers, J.T.; Jiang, Y.L. A mechanistic perspective on the chemistry of DNA repair glycosylases. *Chem. Rev.* **2003**, *103*, 2729–2760. [[CrossRef](#)]
4. Zharkov, D.O.; Grollman, A.P. The DNA trackwalkers: Principles of lesion search and recognition by DNA glycosylases. *Mutat. Res.* **2005**, *577*, 24–54. [[CrossRef](#)] [[PubMed](#)]
5. Lee, A.J.; Wallace, S.S. Hide and seek: How do DNA glycosylases locate oxidatively damaged DNA bases amidst a sea of undamaged bases? *Free Radic. Biol. Med.* **2017**, *107*, 170–178. [[CrossRef](#)]
6. Esadze, A.; Stivers, J.T. Facilitated diffusion mechanisms in DNA base excision repair and transcriptional activation. *Chem. Rev.* **2018**, *118*, 11298–11323. [[CrossRef](#)] [[PubMed](#)]
7. Sousa, M.M.L.; Krokan, H.E.; Slupphaug, G. DNA-uracil and human pathology. *Mol. Asp. Med.* **2007**, *28*, 276–306. [[CrossRef](#)] [[PubMed](#)]
8. Kavli, B.; Slupphaug, G.; Krokan, H.E. Genomic uracil in biology, immunity and cancer. In *DNA Damage, DNA Repair and Disease*; Dizdaroglu, M., Lloyd, R.S., Eds.; Royal Society of Chemistry: London, UK, 2021; Volume 1, pp. 220–248. [[CrossRef](#)]
9. Visnes, T.; Doseth, B.; Pettersen, H.S.; Hagen, L.; Sousa, M.M.L.; Akbari, M.; Otterlei, M.; Kavli, B.; Slupphaug, G.; Krokan, H.E. Uracil in DNA and its processing by different DNA glycosylases. *Philos. Trans. R. Soc. Lond. B Biol. Sci.* **2009**, *364*, 563–568. [[CrossRef](#)]
10. Pyles, R.B.; Thompson, R.L. Evidence that the herpes simplex virus type 1 uracil DNA glycosylase is required for efficient viral replication and latency in the murine nervous system. *J. Virol.* **1994**, *68*, 4963–4972. [[CrossRef](#)]
11. Lu, C.-C.; Huang, H.-T.; Wang, J.-T.; Slupphaug, G.; Li, T.-K.; Wu, M.-C.; Chen, Y.-C.; Lee, C.-P.; Chen, M.-R. Characterization of the uracil-DNA glycosylase activity of Epstein-Barr virus BKRF3 and its role in lytic viral DNA replication. *J. Virol.* **2007**, *81*, 1195–1208. [[CrossRef](#)]
12. Minkah, N.; Macaluso, M.; Oldenburg, D.G.; Paden, C.R.; White, D.W.; McBride, K.M.; Krug, L.T. Absence of the uracil DNA glycosylase of murine gammaherpesvirus 68 impairs replication and delays the establishment of latency in vivo. *J. Virol.* **2015**, *89*, 3366–3379. [[CrossRef](#)]
13. Dong, Q.; Smith, K.R.; Oldenburg, D.G.; Shapiro, M.; Schutt, W.R.; Malik, L.; Plummer, J.B.; Mu, Y.; MacCarthy, T.; White, D.W.; et al. Combinatorial loss of the enzymatic activities of viral uracil-DNA glycosylase and viral dUTPase impairs murine gammaherpesvirus pathogenesis and leads to increased recombination-based deletion in the viral genome. *mBio* **2018**, *9*, e01831-18. [[CrossRef](#)] [[PubMed](#)]
14. Mansky, L.M.; Preveral, S.; Selig, L.; Benarous, R.; Benichou, S. The interaction of Vpr with uracil DNA glycosylase modulates the human immunodeficiency virus type 1 in vivo mutation rate. *J. Virol.* **2000**, *74*, 7039–7047. [[CrossRef](#)] [[PubMed](#)]
15. Chen, R.; Le Rouzic, E.; Kearney, J.A.; Mansky, L.M.; Benichou, S. Vpr-mediated incorporation of UNG2 into HIV-1 particles is required to modulate the virus mutation rate and for replication in macrophages. *J. Biol. Chem.* **2004**, *279*, 28419–28425. [[CrossRef](#)]
16. Guenzel, C.A.; Hérate, C.; Le Rouzic, E.; Maidou-Peindara, P.; Sadler, H.A.; Rouyez, M.-C.; Mansky, L.M.; Benichou, S. Recruitment of the nuclear form of uracil DNA glycosylase into virus particles participates in the full infectivity of HIV-1. *J. Virol.* **2012**, *86*, 2533–2544. [[CrossRef](#)]
17. Stuart, D.T.; Upton, C.; Higman, M.A.; Niles, E.G.; McFadden, G. A poxvirus-encoded uracil DNA glycosylase is essential for virus viability. *J. Virol.* **1993**, *67*, 2503–2512. [[CrossRef](#)]
18. Millns, A.K.; Carpenter, M.S.; DeLange, A.M. The vaccinia virus-encoded uracil DNA glycosylase has an essential role in viral DNA replication. *Virology* **1994**, *198*, 504–513. [[CrossRef](#)] [[PubMed](#)]
19. Ellison, K.S.; Peng, W.; McFadden, G. Mutations in active-site residues of the uracil-DNA glycosylase encoded by vaccinia virus are incompatible with virus viability. *J. Virol.* **1996**, *70*, 7965–7973. [[CrossRef](#)] [[PubMed](#)]
20. Scaramozzino, N.; Sanz, G.; Crance, J.M.; Sapparbaev, M.; Drillien, R.; Laval, J.; Kavli, B.; Garin, D. Characterisation of the substrate specificity of homogeneous vaccinia virus uracil-DNA glycosylase. *Nucleic Acids Res.* **2003**, *31*, 4950–4957. [[CrossRef](#)]
21. Duraffour, S.; Ishchenko, A.A.; Sapparbaev, M.; Crance, J.-M.; Garin, D. Substrate specificity of homogeneous monkeypox virus uracil-DNA glycosylase. *Biochemistry* **2007**, *46*, 11874–11881. [[CrossRef](#)]
22. Schormann, N.; Grigorian, A.; Samal, A.; Krishnan, R.; DeLucas, L.; Chattopadhyay, D. Crystal structure of vaccinia virus uracil-DNA glycosylase reveals dimeric assembly. *BMC Struct. Biol.* **2007**, *7*, 45. [[CrossRef](#)]
23. Druck Shudofsky, A.M.; Silverman, J.E.Y.; Chattopadhyay, D.; Ricciardi, R.P. Vaccinia virus D4 mutants defective in processive DNA synthesis retain binding to A20 and DNA. *J. Virol.* **2010**, *84*, 12325–12335. [[CrossRef](#)] [[PubMed](#)]
24. Sartmatova, D.; Nash, T.; Schormann, N.; Nuth, M.; Ricciardi, R.; Banerjee, S.; Chattopadhyay, D. Crystallization and preliminary X-ray diffraction analysis of three recombinant mutants of *Vaccinia virus* uracil DNA glycosylase. *Acta Crystallogr. Sect. F Struct. Biol. Cryst. Commun.* **2013**, *69*, 295–301. [[CrossRef](#)] [[PubMed](#)]
25. Schormann, N.; Banerjee, S.; Ricciardi, R.; Chattopadhyay, D. Structure of the uracil complex of *Vaccinia virus* uracil DNA glycosylase. *Acta Crystallogr. Sect. F Struct. Biol. Cryst. Commun.* **2013**, *69*, 1328–1334. [[CrossRef](#)] [[PubMed](#)]

26. Contesto-Richefeu, C.; Tarbouriech, N.; Brazzolotto, X.; Betzi, S.; Morelli, X.; Burmeister, W.P.; Iseni, F. Crystal structure of the vaccinia virus DNA polymerase holoenzyme subunit D4 in complex with the A20 N-terminal domain. *PLoS Pathog.* **2014**, *10*, e1003978. [[CrossRef](#)] [[PubMed](#)]
27. Burmeister, W.P.; Tarbouriech, N.; Fender, P.; Contesto-Richefeu, C.; Peyrefitte, C.N.; Iseni, F. Crystal structure of the vaccinia virus uracil-DNA glycosylase in complex with DNA. *J. Biol. Chem.* **2015**, *290*, 17923–17934. [[CrossRef](#)]
28. Schormann, N.; Banerjee, S.; Ricciardi, R.; Chattopadhyay, D. Binding of undamaged double stranded DNA to vaccinia virus uracil-DNA glycosylase. *BMC Struct. Biol.* **2015**, *15*, 10. [[CrossRef](#)]
29. Contesto-Richefeu, C.; Tarbouriech, N.; Brazzolotto, X.; Burmeister, W.P.; Peyrefitte, C.N.; Iseni, F. Structural analysis of point mutations at the *Vaccinia virus* A20/D4 interface. *Acta Crystallogr. F Struct. Biol. Commun.* **2016**, *72*, 687–691. [[CrossRef](#)]
30. Schormann, N.; Zhukovskaya, N.; Bedwell, G.; Nuth, M.; Gillilan, R.; Prevelige, P.E.; Ricciardi, R.P.; Banerjee, S.; Chattopadhyay, D. Poxvirus uracil-DNA glycosylase—An unusual member of the family I uracil-DNA glycosylases. *Protein Sci.* **2016**, *25*, 2113–2131. [[CrossRef](#)]
31. De Silva, F.S.; Moss, B. Vaccinia virus uracil DNA glycosylase has an essential role in DNA synthesis that is independent of its glycosylase activity: Catalytic site mutations reduce virulence but not virus replication in cultured cells. *J. Virol.* **2003**, *77*, 159–166. [[CrossRef](#)]
32. Holzer, G.W.; Falkner, F.G. Construction of a vaccinia virus deficient in the essential DNA repair enzyme uracil DNA glycosylase by a complementing cell line. *J. Virol.* **1997**, *71*, 4997–5002. [[CrossRef](#)]
33. Holzer, G.W.; Gritschenberger, W.; Mayrhofer, J.A.; Wieser, V.; Dorner, F.; Falkner, F.G. Dominant host range selection of vaccinia recombinants by rescue of an essential gene. *Virology* **1998**, *249*, 160–166. [[CrossRef](#)] [[PubMed](#)]
34. Stanitsa, E.S.; Arps, L.; Traktman, P. Vaccinia virus uracil DNA glycosylase interacts with the A20 protein to form a heterodimeric processivity factor for the viral DNA polymerase. *J. Biol. Chem.* **2006**, *281*, 3439–3451. [[CrossRef](#)] [[PubMed](#)]
35. Sidorenko, V.S.; Mechetin, G.V.; Nevinsky, G.A.; Zharkov, D.O. Correlated cleavage of single- and double-stranded substrates by uracil-DNA glycosylase. *FEBS Lett.* **2008**, *582*, 410–414. [[CrossRef](#)]
36. Hedglin, M.; O'Brien, P.J. Human alkyladenine DNA glycosylase employs a processive search for DNA damage. *Biochemistry* **2008**, *47*, 11434–11445. [[CrossRef](#)] [[PubMed](#)]
37. Porecha, R.H.; Stivers, J.T. Uracil DNA glycosylase uses DNA hopping and short-range sliding to trap extrahelical uracils. *Proc. Natl. Acad. Sci. USA* **2008**, *105*, 10791–10796. [[CrossRef](#)]
38. Belotserkovskii, B.P.; Zarlino, D.A. Analysis of a one-dimensional random walk with irreversible losses at each step: Applications for protein movement on DNA. *J. Theor. Biol.* **2004**, *226*, 195–203. [[CrossRef](#)]
39. Sidorenko, V.S.; Zharkov, D.O. Correlated cleavage of damaged DNA by bacterial and human 8-oxoguanine-DNA glycosylases. *Biochemistry* **2008**, *47*, 8970–8976. [[CrossRef](#)]
40. Hedglin, M.; O'Brien, P.J. Hopping enables a DNA repair glycosylase to search both strands and bypass a bound protein. *ACS Chem. Biol.* **2010**, *5*, 427–436. [[CrossRef](#)]
41. Mechetin, G.V.; Zharkov, D.O. Mechanism of translocation of uracil-DNA glycosylase from *Escherichia coli* between distributed lesions. *Biochem. Biophys. Res. Commun.* **2011**, *414*, 425–430. [[CrossRef](#)]
42. Mechetin, G.V.; Zharkov, D.O. The mechanism of substrate search by base excision repair enzymes. *Dokl. Biochem. Biophys.* **2011**, *437*, 94–97. [[CrossRef](#)]
43. Schonhoft, J.D.; Stivers, J.T. Timing facilitated site transfer of an enzyme on DNA. *Nat. Chem. Biol.* **2012**, *8*, 205–210. [[CrossRef](#)]
44. Hedglin, M.; Zhang, Y.; O'Brien, P.J. Isolating contributions from intersegmental transfer to DNA searching by alkyladenine DNA glycosylase. *J. Biol. Chem.* **2013**, *288*, 24550–24559. [[CrossRef](#)]
45. Schonhoft, J.D.; Kosowicz, J.G.; Stivers, J.T. DNA translocation by human uracil DNA glycosylase: Role of DNA phosphate charge. *Biochemistry* **2013**, *52*, 2526–2535. [[CrossRef](#)] [[PubMed](#)]
46. Schonhoft, J.D.; Stivers, J.T. DNA translocation by human uracil DNA glycosylase: The case of single-stranded DNA and clustered uracils. *Biochemistry* **2013**, *52*, 2536–2544. [[CrossRef](#)] [[PubMed](#)]
47. Rowland, M.M.; Schonhoft, J.D.; McKibbin, P.L.; David, S.S.; Stivers, J.T. Microscopic mechanism of DNA damage searching by hOGG1. *Nucleic Acids Res.* **2014**, *42*, 9295–9303. [[CrossRef](#)] [[PubMed](#)]
48. Cravens, S.L.; Schonhoft, J.D.; Rowland, M.M.; Rodriguez, A.A.; Anderson, B.G.; Stivers, J.T. Molecular crowding enhances facilitated diffusion of two human DNA glycosylases. *Nucleic Acids Res.* **2015**, *43*, 4087–4097. [[CrossRef](#)]
49. Hedglin, M.; Zhang, Y.; O'Brien, P.J. Probing the DNA structural requirements for facilitated diffusion. *Biochemistry* **2015**, *54*, 557–566. [[CrossRef](#)]
50. Cravens, S.L.; Stivers, J.T. Comparative effects of ions, molecular crowding, and bulk DNA on the damage search mechanisms of hOGG1 and hUNG. *Biochemistry* **2016**, *55*, 5230–5242. [[CrossRef](#)]
51. Esadze, A.; Rodriguez, G.; Weiser, B.P.; Cole, P.A.; Stivers, J.T. Measurement of nanoscale DNA translocation by uracil DNA glycosylase in human cells. *Nucleic Acids Res.* **2017**, *45*, 12413–12424. [[CrossRef](#)]
52. Mechetin, G.V.; Dyatlova, E.A.; Sinyakov, A.N.; Ryabinin, V.A.; Vorobjev, P.E.; Zharkov, D.O. Correlated target search by uracil-DNA glycosylase in the presence of bulky adducts and DNA-binding ligands. *Russ. J. Bioorg. Chem.* **2017**, *43*, 23–28. [[CrossRef](#)]
53. Rodriguez, G.; Esadze, A.; Weiser, B.P.; Schonhoft, J.D.; Cole, P.A.; Stivers, J.T. Disordered N-terminal domain of human uracil DNA glycosylase (hUNG2) enhances DNA translocation. *ACS Chem. Biol.* **2017**, *12*, 2260–2263. [[CrossRef](#)] [[PubMed](#)]



54. Berg, O.G.; Winter, R.B.; von Hippel, P.H. Diffusion-driven mechanisms of protein translocation on nucleic acids. 1. Models and theory. *Biochemistry* **1981**, *20*, 6929–6948. [[CrossRef](#)]
55. Winter, R.B.; von Hippel, P.H. Diffusion-driven mechanisms of protein translocation on nucleic acids. 2. The *Escherichia coli* repressor–operator interaction: Equilibrium measurements. *Biochemistry* **1981**, *20*, 6948–6960. [[CrossRef](#)] [[PubMed](#)]
56. Winter, R.B.; Berg, O.G.; von Hippel, P.H. Diffusion-driven mechanisms of protein translocation on nucleic acids. 3. The *Escherichia coli* lac repressor–operator interaction: Kinetic measurements and conclusions. *Biochemistry* **1981**, *20*, 6961–6977. [[CrossRef](#)] [[PubMed](#)]
57. Owczarzy, R.; Moreira, B.G.; You, Y.; Behlke, M.A.; Walder, J.A. Predicting stability of DNA duplexes in solutions containing magnesium and monovalent cations. *Biochemistry* **2008**, *47*, 5336–5353. [[CrossRef](#)]
58. Slupphaug, G.; Eftedal, I.; Kavli, B.; Bharati, S.; Helle, N.M.; Haug, T.; Levine, D.W.; Krokan, H.E. Properties of a recombinant human uracil–DNA glycosylase from the UNG gene and evidence that UNG encodes the major uracil–DNA glycosylase. *Biochemistry* **1995**, *34*, 128–138. [[CrossRef](#)]
59. Kavli, B.; Sundheim, O.; Akbari, M.; Otterlei, M.; Nilsen, H.; Skorpen, F.; Aas, P.A.; Hagen, L.; Krokan, H.E.; Slupphaug, G. hUNG2 is the major repair enzyme for removal of uracil from U:A matches, U:G mismatches, and U in single-stranded DNA, with hSMUG1 as a broad specificity backup. *J. Biol. Chem.* **2002**, *277*, 39926–39936. [[CrossRef](#)]
60. Blainey, P.C.; Luo, G.; Kou, S.C.; Mangel, W.F.; Verdine, G.L.; Bagchi, B.; Xie, X.S. Nonspecifically bound proteins spin while diffusing along DNA. *Nat. Struct. Mol. Biol.* **2009**, *16*, 1224–1229. [[CrossRef](#)]
61. Stivers, J.T.; Pankiewicz, K.W.; Watanabe, K.A. Kinetic mechanism of damage site recognition and uracil flipping by *Escherichia coli* uracil DNA glycosylase. *Biochemistry* **1999**, *38*, 952–963. [[CrossRef](#)]
62. Grin, I.R.; Mechetin, G.V.; Kasymov, R.D.; Diatlova, E.A.; Yudkina, A.V.; Shchelkunov, S.N.; Gileva, I.P.; Denisova, A.A.; Stepanov, G.A.; Chilov, G.G.; et al. A new class of uracil–DNA glycosylase inhibitors active against human and vaccinia virus enzyme. *Molecules* **2021**, *26*, 6668. [[CrossRef](#)]
63. Wu, X.; Zhang, Y. TET-mediated active DNA demethylation: Mechanism, function and beyond. *Nat. Rev. Genet.* **2017**, *18*, 517–534. [[CrossRef](#)] [[PubMed](#)]
64. Parrilla-Doblas, J.T.; Roldán-Arjona, T.; Ariza, R.R.; Córdoba-Cañero, D. Active DNA demethylation in plants. *Int. J. Mol. Sci.* **2019**, *20*, 4683. [[CrossRef](#)] [[PubMed](#)]
65. Wang, R.; Hao, W.; Pan, L.; Boldogh, I.; Ba, X. The roles of base excision repair enzyme OGG1 in gene expression. *Cell. Mol. Life Sci.* **2018**, *75*, 3741–3750. [[CrossRef](#)] [[PubMed](#)]
66. Hedglin, M.; Kumar, R.; Benkovic, S.J. Replication clamps and clamp loaders. *Cold Spring Harb. Perspect. Biol.* **2013**, *5*, a010165. [[CrossRef](#)]
67. Zuccola, H.J.; Filman, D.J.; Coen, D.M.; Hogle, J.M. The crystal structure of an unusual processivity factor, herpes simplex virus UL42, bound to the C terminus of its cognate polymerase. *Mol. Cell* **2000**, *5*, 267–278. [[CrossRef](#)]
68. Appleton, B.A.; Loregian, A.; Filman, D.J.; Coen, D.M.; Hogle, J.M. The cytomegalovirus DNA polymerase subunit UL44 forms a C clamp-shaped dimer. *Mol. Cell* **2004**, *15*, 233–244. [[CrossRef](#)]
69. Huber, H.E.; Tabor, S.; Richardson, C.C. *Escherichia coli* thioredoxin stabilizes complexes of bacteriophage T7 DNA polymerase and primed templates. *J. Biol. Chem.* **1987**, *262*, 16224–16232. [[CrossRef](#)]
70. Doublé, S.; Tabor, S.; Long, A.M.; Richardson, C.C.; Ellenberger, T. Crystal structure of a bacteriophage T7 DNA replication complex at 2.2 Å resolution. *Nature* **1998**, *391*, 251–258. [[CrossRef](#)]
71. Gao, Y.; Cui, Y.; Fox, T.; Lin, S.; Wang, H.; de Val, N.; Zhou, H.; Yang, W. Structures and operating principles of the replisome. *Science* **2019**, *363*, eaav7003. [[CrossRef](#)]
72. Foster, B.M.; Rosenberg, D.; Salvo, H.; Stephens, K.L.; Bintz, B.J.; Hammel, M.; Ellenberger, T.; Gainey, M.D.; Wallen, J.R. Combined solution and crystal methods reveal the electrostatic tethers that provide a flexible platform for replication activities in the bacteriophage T7 replisome. *Biochemistry* **2019**, *58*, 4466–4479. [[CrossRef](#)]
73. Sun, S.; Geng, L.; Shamoo, Y. Structure and enzymatic properties of a chimeric bacteriophage RB69 DNA polymerase and single-stranded DNA binding protein with increased processivity. *Proteins* **2006**, *65*, 231–238. [[CrossRef](#)] [[PubMed](#)]
74. Olszewski, M.; Śpibida, M.; Bilek, M.; Krawczyk, B. Fusion of *Taq* DNA polymerase with single-stranded DNA binding-like protein of *Nanoarchaeum equitans*—Expression and characterization. *PLoS ONE* **2017**, *12*, e0184162. [[CrossRef](#)] [[PubMed](#)]
75. Wang, Y.; Prosen, D.E.; Mei, L.; Sullivan, J.C.; Finney, M.; Vander Horn, P.B. A novel strategy to engineer DNA polymerases for enhanced processivity and improved performance in vitro. *Nucleic Acids Res.* **2004**, *32*, 1197–1207. [[CrossRef](#)] [[PubMed](#)]
76. de Vega, M.; Lázaro, J.M.; Mencía, M.; Blanco, L.; Salas, M. Improvement of  $\phi$ 29 DNA polymerase amplification performance by fusion of DNA binding motifs. *Proc. Natl. Acad. Sci. USA* **2010**, *107*, 16506–16511. [[CrossRef](#)] [[PubMed](#)]
77. Pavlov, A.R.; Pavlova, N.V.; Kozyavkin, S.A.; Slesarev, A.I. Cooperation between catalytic and DNA binding domains enhances thermostability and supports DNA synthesis at higher temperatures by thermostable DNA polymerases. *Biochemistry* **2012**, *51*, 2032–2043. [[CrossRef](#)]
78. McDonald, W.F.; Traktman, P. Vaccinia virus DNA polymerase: *In vitro* analysis of parameters affecting processivity. *J. Biol. Chem.* **1994**, *269*, 31190–31197. [[CrossRef](#)]
79. McDonald, W.F.; Klemperer, N.; Traktman, P. Characterization of a processive form of the vaccinia virus DNA polymerase. *Virology* **1997**, *234*, 168–175. [[CrossRef](#)]
80. Moss, B. Poxvirus DNA replication. *Cold Spring Harb. Perspect. Biol.* **2013**, *5*, a010199. [[CrossRef](#)]

81. Greseth, M.D.; Traktman, P. The life cycle of the vaccinia virus genome. *Annu. Rev. Virol.* **2022**, *9*, 239–259. [[CrossRef](#)]
82. Boyle, K.A.; Stanitsa, E.S.; Greseth, M.D.; Lindgren, J.K.; Traktman, P. Evaluation of the role of the vaccinia virus uracil DNA glycosylase and A20 proteins as intrinsic components of the DNA polymerase holoenzyme. *J. Biol. Chem.* **2011**, *286*, 24702–24713. [[CrossRef](#)]
83. Sèle, C.; Gabel, F.; Gutsche, I.; Ivanov, I.; Burmeister, W.P.; Iseni, F.; Tarbouriech, N. Low-resolution structure of vaccinia virus DNA replication machinery. *J. Virol.* **2013**, *87*, 1679–1689. [[CrossRef](#)] [[PubMed](#)]
84. Peng, Q.; Xie, Y.; Kuai, L.; Wang, H.; Qi, J.; Gao, G.F.; Shi, Y. Structure of monkeypox virus DNA polymerase holoenzyme. *Science* **2023**, *379*, 100–105. [[CrossRef](#)] [[PubMed](#)]
85. Lu, H.; Zhou, Q.; He, J.; Jiang, Z.; Peng, C.; Tong, R.; Shi, J. Recent advances in the development of protein–protein interactions modulators: Mechanisms and clinical trials. *Signal Transduct. Target. Ther.* **2020**, *5*, 213. [[CrossRef](#)] [[PubMed](#)]
86. Schormann, N.; Sommers, C.I.; Prichard, M.N.; Keith, K.A.; Noah, J.W.; Nuth, M.; Ricciardi, R.P.; Chattopadhyay, D. Identification of protein-protein interaction inhibitors targeting vaccinia virus processivity factor for development of antiviral agents. *Antimicrob. Agents Chemother.* **2011**, *55*, 5054–5062. [[CrossRef](#)]
87. Nuth, M.; Huang, L.; Saw, Y.L.; Schormann, N.; Chattopadhyay, D.; Ricciardi, R.P. Identification of inhibitors that block vaccinia virus infection by targeting the DNA synthesis processivity factor D4. *J. Med. Chem.* **2011**, *54*, 3260–3267. [[CrossRef](#)]
88. Nuth, M.; Guan, H.; Zhukovskaya, N.; Saw, Y.L.; Ricciardi, R.P. Design of potent poxvirus inhibitors of the heterodimeric processivity factor required for viral replication. *J. Med. Chem.* **2013**, *56*, 3235–3246. [[CrossRef](#)]
89. Guan, H.; Nuth, M.; Zhukovskaya, N.; Saw, Y.L.; Bell, E.; Isaacs, S.N.; Ricciardi, R.P. A novel target and approach for identifying antivirals against molluscum contagiosum virus. *Antimicrob. Agents Chemother.* **2014**, *58*, 7383–7389. [[CrossRef](#)]
90. Nuth, M.; Guan, H.; Xiao, Y.; Kulp, J.L., 3rd; Parker, M.H.; Strobel, E.D.; Isaacs, S.N.; Scott, R.W.; Reitz, A.B.; Ricciardi, R.P. Mutation and structure guided discovery of an antiviral small molecule that mimics an essential C-terminal tripeptide of the vaccinia D4 processivity factor. *Antivir. Res.* **2019**, *162*, 178–185. [[CrossRef](#)]
91. Gruskin, E.A.; Lloyd, R.S. Molecular analysis of plasmid DNA repair within ultraviolet-irradiated Escherichia coli. I. T4 endonuclease V-initiated excision repair. *J. Biol. Chem.* **1988**, *263*, 12728–12737. [[CrossRef](#)]
92. Beattie, T.R.; Kapadia, N.; Nicolas, E.; Uphoff, S.; Wollman, A.J.M.; Leake, M.C.; Reyes-Lamothe, R. Frequent exchange of the DNA polymerase during bacterial chromosome replication. *Life* **2017**, *6*, e21763. [[CrossRef](#)]
93. Yakubitskiy, S.N.; Kolosova, I.V.; Maksyutov, R.A.; Shchelkunov, S.N. Attenuation of vaccinia virus. *Acta Nat.* **2015**, *7*, 113–121. [[CrossRef](#)]
94. Gasteiger, E.; Jung, E.; Bairoch, A. SWISS-PROT: Connecting biomolecular knowledge via a protein database. *Curr. Issues Mol. Biol.* **2001**, *3*, 47–55. [[CrossRef](#)] [[PubMed](#)]
95. Huang, C.Y. Derivation of initial velocity and isotope exchange rate equations. *Methods Enzymol.* **1979**, *63*, 54–84. [[CrossRef](#)] [[PubMed](#)]

**Disclaimer/Publisher’s Note:** The statements, opinions and data contained in all publications are solely those of the individual author(s) and contributor(s) and not of MDPI and/or the editor(s). MDPI and/or the editor(s) disclaim responsibility for any injury to people or property resulting from any ideas, methods, instructions or products referred to in the content.